

An Efficient Search for Gravitationally-Lensed Radio Lobes

Submitted to ApJ: 2000.07.28.

J. Lehar¹, A. Buchalter², R.G. McMahon³, C.S. Kochanek¹, T.W.B. Muxlow⁴

ABSTRACT

We performed an automated comparison of the FIRST radio survey with the APM optical catalog to find radio lobes with optical counterparts. Based on an initial survey covering ~ 3000 square degrees, we selected a sample of 33 lens candidates for VLA confirmation. VLA and optical observations of these candidates yielded two confirmed lens systems, one a new discovery (J0816+5003), and one of which was previously known (J1549+3047). Three other candidates have radio lobes with galaxies superposed, but lack evidence of multiple imaging. One of these targets (J0958+2846) is a projected close pair of quasars ($8''$ separation at redshifts 2.064 and 2.744). Our search method is highly efficient, with $>5\%$ of our observing targets being lensed, compared to the usual success rate of $<1\%$. Using the whole FIRST survey, we expect to find ~ 10 lenses in short order using this approach, and the sample could increase to hundreds of lensed lobes in the Northern sky, using deeper optical surveys and planned upgrades to the VLA. Such a sample would be a powerful probe of galaxy structure and evolution.

Subject headings: Gravitational Lenses — Dark Matter — Cosmology

1. Introduction

The 60 known gravitational lenses are powerful astrophysical probes. They are the only galaxies selected on mass rather than luminosity, making them a unique sample with very different properties and biases from traditional luminosity-selected galaxies. All lenses have extraordinarily precise mass measurements (better than 5% including systematics), allowing detailed comparisons of galaxies of constant mass. Lensing has been used to constrain cosmological parameters (see reviews by Schneider et al. 1992; Blandford & Narayan 1992), the structure and evolution of galaxies (e.g., Keeton et al. 1997, Keeton et al. 1998, Kochanek et al. 2000), quasar and AGN host galaxies

¹ Center for Astrophysics, 60 Garden St, Cambridge, MA 02138, USA, jlehar@cfa.harvard.edu.

² Theoretical Astrophysics Group, Caltech, 130-33, Pasadena, CA 91125, ari@tapir.caltech.edu

³ Institute of Astronomy, Madingley Rd, Cambridge, CB3 0HA, UK

⁴ Nuffield Radio Astronomy Laboratories, Jodrell Bank, Cheshire SK11 9DL, UK

(e.g., Keeton et al. 2000), and even the interstellar medium and extinction in intermediate-redshift galaxies (e.g., Falco et al. 1999).

Such astrophysical studies are limited by the sample size. The properties of each individual lens depend on many variables, e.g., the source redshift, the lens redshift, the galaxy mass, and the position of the source behind the lens. With only 60 lenses known, it is difficult to subdivide the sample over more than one variable. For example, the ~ 30 lenses used in galaxy evolution studies allow only 4 redshift bins of roughly 8 galaxies each. Thus, one cannot separately explore the evolution of high and low mass galaxies, or the average mass or number density of the lenses in each bin. Only 10–20% of lenses are produced by spiral galaxies (e.g. Fukugita & Turner 1991), so hundreds of lensed systems must be found to provide an adequate statistical sample of spiral galaxy lenses.

Fortunately, there is no shortage of undiscovered lenses. Statistical estimates suggest that there are 0.5 lenses per square degree for a quasar sample complete to about $V=24$ (Kochanek 1996a), or for radio sources with 5 GHz radio flux of >10 mJy (Kochanek 1996b). Equivalently, 1–10 in 1000 sources with redshifts above unity will be gravitationally lensed depending on the type of source and its flux. The problem is finding them in an *efficient* manner.

The first surveys for lenses focused on bright quasars (see Blandford & Narayan 1992), with a discovery rate of roughly 1 per 100–200 targets. The high rate is due to the effects of magnification bias (Turner 1990), which is important for all lens samples but critical for surveys of bright quasars. This strategy is limited by the relative rarity of bright quasars, the difficulty of obtaining large numbers of high resolution optical images, and contamination from stars.

Another successful strategy was to look for lensed radio sources. Extra-galactic radio sources are numerous and distant, and confusing low-redshift sources are rare. The three largest radio searches, MG-VLA (Burke et al.1993), JVAS (Patnaik et al.1992; Patnaik 1993) and CLASS (Jackson et al.1997), have discovered almost half of the ~ 60 known galaxy-mass lenses. Their strategy was to image all radio sources to a fixed flux limit, and then use the morphology of each radio image to identify the lenses. Typically, one lensed radio source is discovered for every 500 survey targets. Radio searches also led to the discovery of an important new class of lenses where the lensed images of an extended background source merge to form an “Einstein ring” of emission around the lens galaxy (e.g., Hewitt et al.1988). Unlike a compact source, an extended background source probes many lines of sight which extend well into the halo of the lens, allowing much better constraints on the dark-matter profile (e.g., Kochanek 1995).

In this paper, we present an efficient search for lensed radio lobes using combined radio and optical surveys. The survey selection is outlined in §2, and follow-up observations are described in §3. In §5, we discuss individual candidates for lensing, and in §6, we summarize our conclusions.

2. The FIRST-APM Lensed Lobe Search

Most lensed radio sources are being missed by present searches. Powerful radio galaxies are often flanked by two extended radio lobes, whose radio spectrum is markedly steeper than that of the compact core (e.g. FR-type objects; Fanaroff & Riley 1974). Due to their extended nature, the optical depth to lensing of such lobes is significantly higher than for unresolved sources. Indeed, the typical lobe size of a few arcseconds implies that $\sim 70\%$ of lensed radio sources should be lobes (Kochanek & Lawrence 1990). The JVAS and CLASS surveys select only flat-spectrum radio sources, and thus lobes constitute only $\sim 20\%$ of their lenses. The smaller MG-VLA search found more lensed lobes ($\sim 50\%$ of lenses), but still missed a significant number. Many lensed lobes are simply not recognized, because the background source itself often has complicated structure, and often lacks sharp features which can produce a clear lensing signature. Sensitive, high-resolution radio maps are required to identify lensed structures ($\sim 1''$ scale) in these cases.

Lensed lobes can be found efficiently because they usually lie *outside* their host galaxy. Radio-galaxy hosts are centered on their compact cores, so radio lobes should not have direct optical counterparts. A galaxy which coincides with a radio lobe is almost certainly a chance alignment, and the relative distances of radio and optical sources strongly favors the galaxy being a foreground lens (Kochanek & Lawrence 1990). Clear examples of this phenomenon were found in the MG-VLA search (MG J1654+1346, Langston et al.1989; MG J1549+3047, Lehar et al.1993). Thus, an efficient way to find lenses is to identify radio lobes with superposed optical galaxies.

A useful sample of radio lobes requires a large, low frequency, radio survey with sufficient angular resolution to distinguish lobes from cores. The VLA⁵ FIRST Survey⁶ (Becker, White, & Helfand 1995), has a flux sensitivity of 1 mJy (6σ) at 20 cm, $5''$ resolution (FWHM) and sub-arcsecond positional accuracy. This represents a factor of ~ 50 improvement in both sensitivity and resolution over previous large-area surveys. At the time of our initial lens search, the northern FIRST sample covered ~ 3000 square degrees ($7^h < \text{RA} < 18^h$ and $22^\circ < \text{DEC} < 58^\circ$), and comprised $\sim 3 \times 10^5$ radio components. To determine the maximum possible sample size using this approach, we searched the full FIRST catalog for lensed-lobe candidates, even though most of them are too faint to be followed up, with high resolution radio observations, at present, due to their steep spectra and extended structures.

A good sample of optical counterparts is provided by the APM⁷ catalog (McMahon & Irwin 1992; Maddox et al.1990), based on the Palomar Observatory Sky Survey plates (POSS-I). The POSS-I plates have a detection limit of $R \sim 20$, and we conservatively estimate that 25–35% of the

⁵ The Very Large Array (VLA) is an NRAO facility. The NRAO is operated by Associated Universities, Inc., under cooperative agreement with the National Science Foundation.

⁶see <http://sundog.stsci.edu/>

⁷ The Automatic Plate Measuring (APM) machine is a National Astronomy Facility run by the Institute of Astronomy in Cambridge, UK (see <http://www.ast.cam.ac.uk/~apmcat>).

known lens galaxies (see Keeton et al.1998) are bright enough to be included in the APM catalog.

2.1. Survey Selection

For the FIRST-APM lensed lobe search, we combined these two surveys to find optical counterparts to radio lobes. We classified the FIRST sources by their radio morphology, and identified those components most likely to be lobes. We then identified as lens candidates those radio lobes with APM counterparts. The estimated mean redshift of FIRST sources is $\langle z \rangle \sim 1$ (Cress & Kamionkowski 1998), and the measured redshift distribution of optical surveys such as the APM Galaxy Survey peaks at $\langle z \rangle \sim 0.12$ (Baugh & Efstathiou 1993). Thus it is likely that APM counterparts to FIRST radio lobes are indeed in the foreground, and potentially lenses.

To define a radio-lobe sample, it is necessary to first “collapse” the radio catalog, such that multiple components of a single radio source are associated with each other. The collapse algorithm is described fully in the Appendix. We ran the collapse routine using a $60''$ search radius, a maximum component separation of $90''$ for triples and multiples (defined as sources with more than three components), and a 10% random association probability cutoff, $P < 0.1$. For ease of detection and phase calibration in follow-up radio observations, we required all component fluxes to exceed 3 mJy, and at least one component to exceed 10 mJy. To enhance selection of true, FR-type doubled-lobed objects, we required a symmetry factor of $S > 0.5$ for triples (where S is defined as the ratio of the shorter core-to-lobe distance to the longer), and a bending angle of $\theta < 30^\circ$ for triples and multiples (see Figure 10 in Appendix). The output of the routine is a list, containing positional, flux, and morphological data, of collapsed radio sources containing two, three, or more components, each of which is identified as either a “core” or a “lobe.” Due to the wide array of radio-source morphologies (core-jet, double-lobed, cometary, diffuse, etc.) and the limited resolution of FIRST, there is no simple, obvious manner in which one can correctly and unambiguously collapse all sources. The parameters we have chosen yield a reasonable balance between ensuring an accurate correspondence between collapsed and real sources, and are in good agreement with the conclusions of “by-eye” inspections (D. Helfand, private communication).

The APM-counterpart selection was as follows. For every collapsed FIRST source, we searched for optical counterparts to each lobe component, as well as to the core component (or to the source centroid, if no radio core was identified) Optical objects were taken to be coincident with a radio component if they fell inside an ellipse defined by the FWHM major and minor axes of the radio component, as listed in the FIRST catalog. For cases where the cataloged major and/or minor axis was less than $2''$, we adopted an effective FWHM value of $2''$ for that axis. For sources without a radio core, optical objects that fell within $\ell/4$ from the average component position were considered core counterparts (where ℓ is the maximum component separation). Those sources with at least one optical counterpart to a radio lobe, which was not also a counterpart to the radio core, became candidates for lensing. We eliminated candidates in which a single optical counterpart matched to both lobe components of a double radio source, as these usually corresponded to identifications of

the host galaxy; for the same reason, we also eliminated cases where a double or multiple source was found to have only one match, corresponding to a compact FIRST component. To ensure sufficient contrast for lensing signatures, we eliminated all candidate lensed lobes larger than $10''$ (FWHM), and further eliminated all candidates whose lobe counterparts fell farther than $2''$ from the fitted peak of the radio lobe. Each lobe counterpart was assigned a letter classification (Table 1) to indicate its likelihood of being a lens, based on its APM color and morphology.

There were 1037 candidates in our sample, each of which has an APM object within $2''$ of a presumed FIRST lobe's peak. The selection methods applied to the radio lobe and counterpart samples are summarized in Table 2. With about one lens candidate for every ~ 200 independent FIRST sources, our candidate selection rate using our chosen criteria is roughly twice the discovery rate for earlier radio lens searches, which suggests that many of our candidates are not lensed. Only about 14% of the candidates have core detections, compared to the much higher 40% POSS-I identification rate for MG-VLA lobed radio sources (Lehár 1991), partly because of the higher MG-VLA flux cutoff (60 mJy at 6 cm), but also because many lensed-lobe candidates are themselves misidentified radio cores. The lensed-lobe candidate and FIRST counterpart distributions are similar, and both have more red, extended objects than the APM catalog in general (see Table 1), probably because both radio samples preferentially select galaxies. There are a large number of blue lobe counterparts, many of which are radio cores with quasar counterparts. However, 62% of these blue counterparts have uncertain optical identifications, because they are close to blue POSS-I detection limit and are absent in the red catalog.

2.2. The VLA Sample

Because of the limited angular resolution of FIRST ($\sim 5''$ FWHM), higher-resolution radio observations are needed to confirm candidates as lensed. Most radio lobes extend over only a few arcseconds, so FIRST cannot always determine unambiguously which components associated with a source are truly radio lobes, and which are compact cores. Moreover, the typical image separation, $\Delta\theta$, for galaxy-mass lenses is only $\sim 1''$, so the effects of lensing cannot be seen directly in the FIRST images. The VLA can achieve sufficient angular resolution to distinguish lobes and resolve gravitational lensing, but only by observing at shorter wavelengths (A-array resolution $\sim 0.4''$ at 6 cm).

Since radio lobes generally have very steep radio spectra, the reduced source flux at shorter wavelengths drastically reduces the number of lens candidates accessible to short, high-resolution VLA observations. The lensed radio lobe in MG J1549+3047 (Lehár et al. 1993) is typical of what we expect to find in our lensed lobe search, in that only fainter parts of the lobe are multiply imaged by an off-center lens galaxy. The lensed lobe has a FIRST flux density of 877 mJy, but at 6 cm the total flux density is 200 mJy, with the hot spots peaking at only 16 mJy per beam. The mean surface brightness of the lensed ring is much fainter (typically ~ 2 mJy/beam), but can be detected with a signal-to-noise ratio of 3 in a 1.5 minute VLA observation. If our lensed lobes have

similar properties, lensing signatures should be detectable in 30 minute observations for FIRST lobes exceeding 200 mJy. A lensed lobe like that in MG J1549+3047, but with a FIRST flux of 100 mJy, would require a 2 hr VLA 6 cm observation for reliable ring detection. Much shorter observations, however, would suffice to rule out cases where we had misidentified a compact core as a lobe.

With these considerations, we selected a small sample of lensed-lobe candidates for VLA confirmation. There were 78 lensed-lobe candidates with FIRST flux > 100 mJy. The limited VLA schedule forced us to choose a subsample of these targets, and this was done by visual inspection. By comparing the FIRST maps to POSS-I fields from the Digitized Sky Survey (DSS⁸), two of us (AB and JL) visually ranked each of the 78 candidates by likelihood of lensing, based on optical colors, radio morphology, alignment, and so on. We compared notes on our rankings and eliminated those candidates that seemed unlikely to be lensed (e.g., candidates which had a single APM counterpart corresponding to a fairly compact component between two others).

Our final VLA sample of 33 candidates is listed in Table 3, and, as a visual guide, Figure 1 presents FIRST cutout maps, with optical fields from the DSS. Since the DSS astrometry can be in error by a few arcseconds, we registered the DSS images to the APM catalog, whose absolute positions deviate by $< 0''.5$ for small objects. This was done by selecting ~ 20 APM objects in each DSS field and finding the least-squares linear coordinate transformation (internal residuals were typically less than $0''.5$). The FIRST maps were superposed using the VLA phase calibrator astrometry which routinely yields $\sim 0''.2$ positional accuracy.

3. Observations

Most of the FIRST/APM lensed-lobe candidates are expected to be radio cores which had been misidentified as lobes, or genuine radio lobes with stellar or nonexistent counterparts (APM/POSS artefacts). To eliminate such cases, and to establish remaining gravitational lens candidates, we obtained higher quality radio and optical observations. We used archival data where available, but the bulk of our targets required new observations. The observations we used are summarized in Table 4, and will be referred to by the labels therein.

We obtained VLA observations for the entire accessible sample (Table 3). Eight of our targets had appropriate archival observations, but most were observed using the A-array at 6 cm (r98b, see Table 4). The total allocation of 8 hours, was divided between the targets based on the lobe flux (see Table 3). Calibrators were observed every ~ 15 min to ensure proper phase calibration,

⁸ Based on photographic data of the National Geographic Society – Palomar Geographic Society to the California Institute of Technology. The plates were processed into the present compressed digital form with their permission. The Digitized Sky Survey was produced at the Space Telescope Science Institute under US Government grant NAG W-2166.

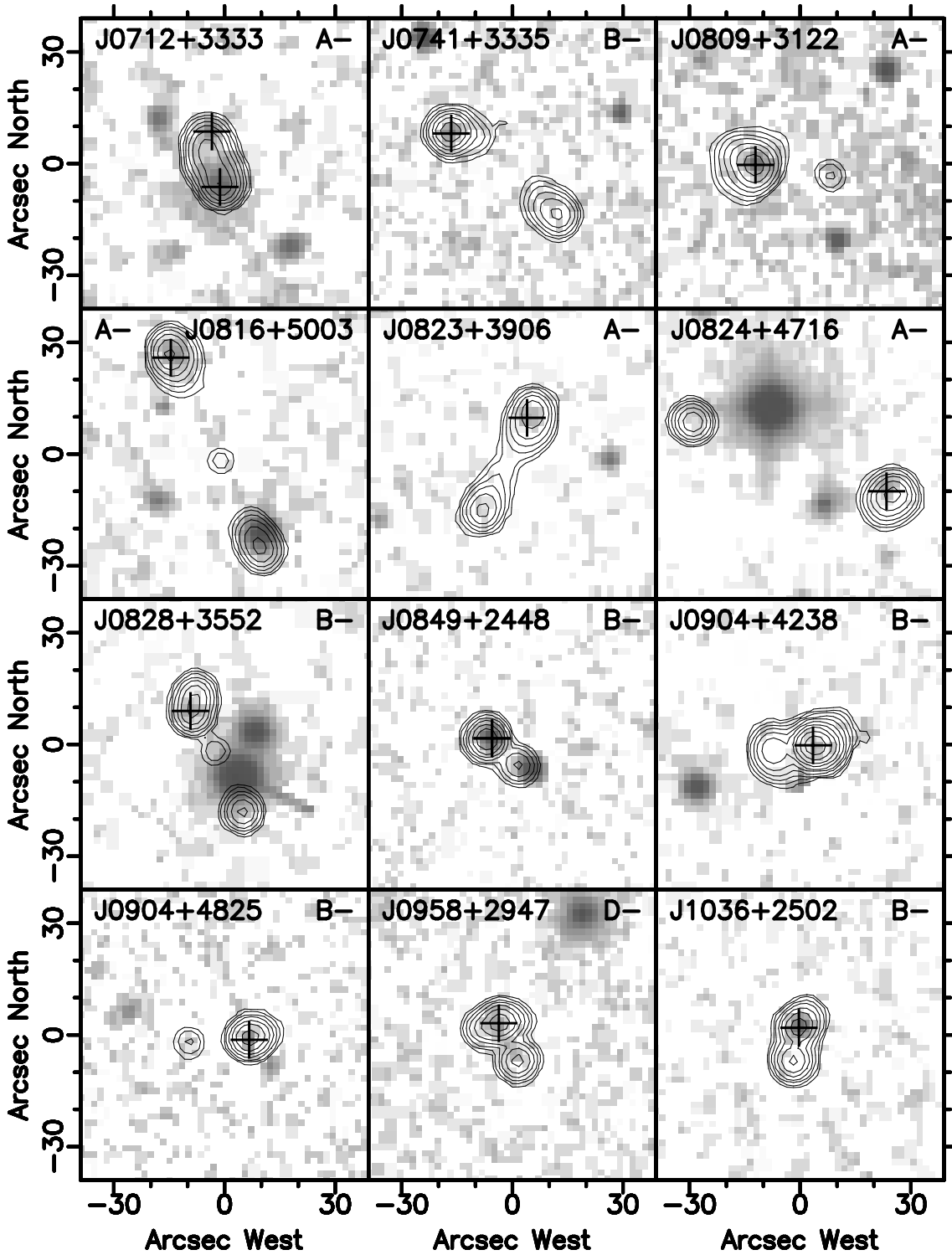


Fig. 1.— VLA sample of lensed-lobe candidates with the lobe counterpart’s optical class (Table 1), FIRST radio maps and DSS optical fields. Radio contours increase by doubling from 1 mJy/beam; and the grey scale map shows the logarithm of DSS optical brightness. APM counterparts to FIRST components are marked by crosshairs. A few blue APM counterparts are not seen on the DSS. The maps were aligned using APM astrometry, and are centered on the positions given in Table 3.

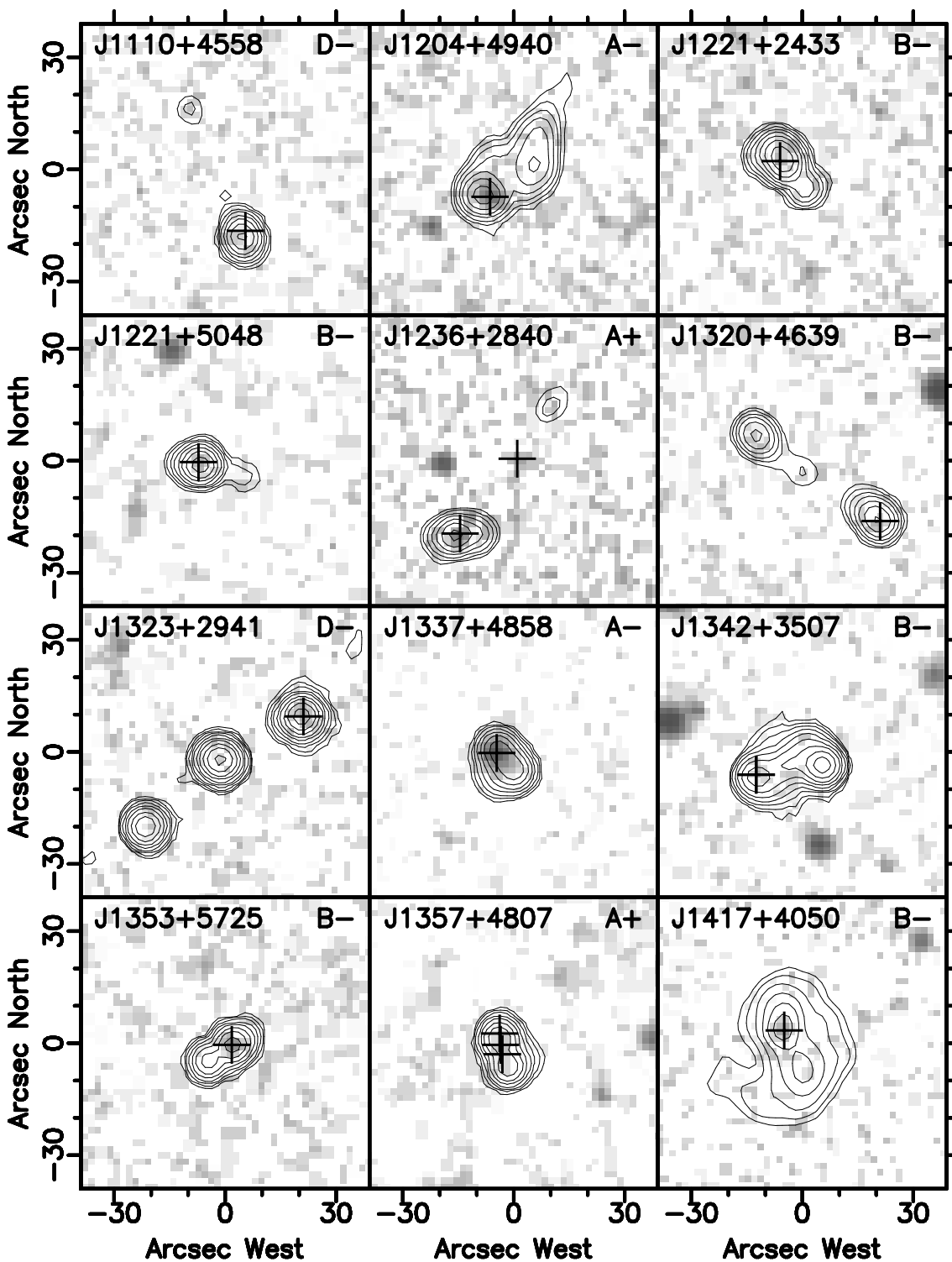


Fig. 1.— More FIRST/DSS maps of the VLA sample.

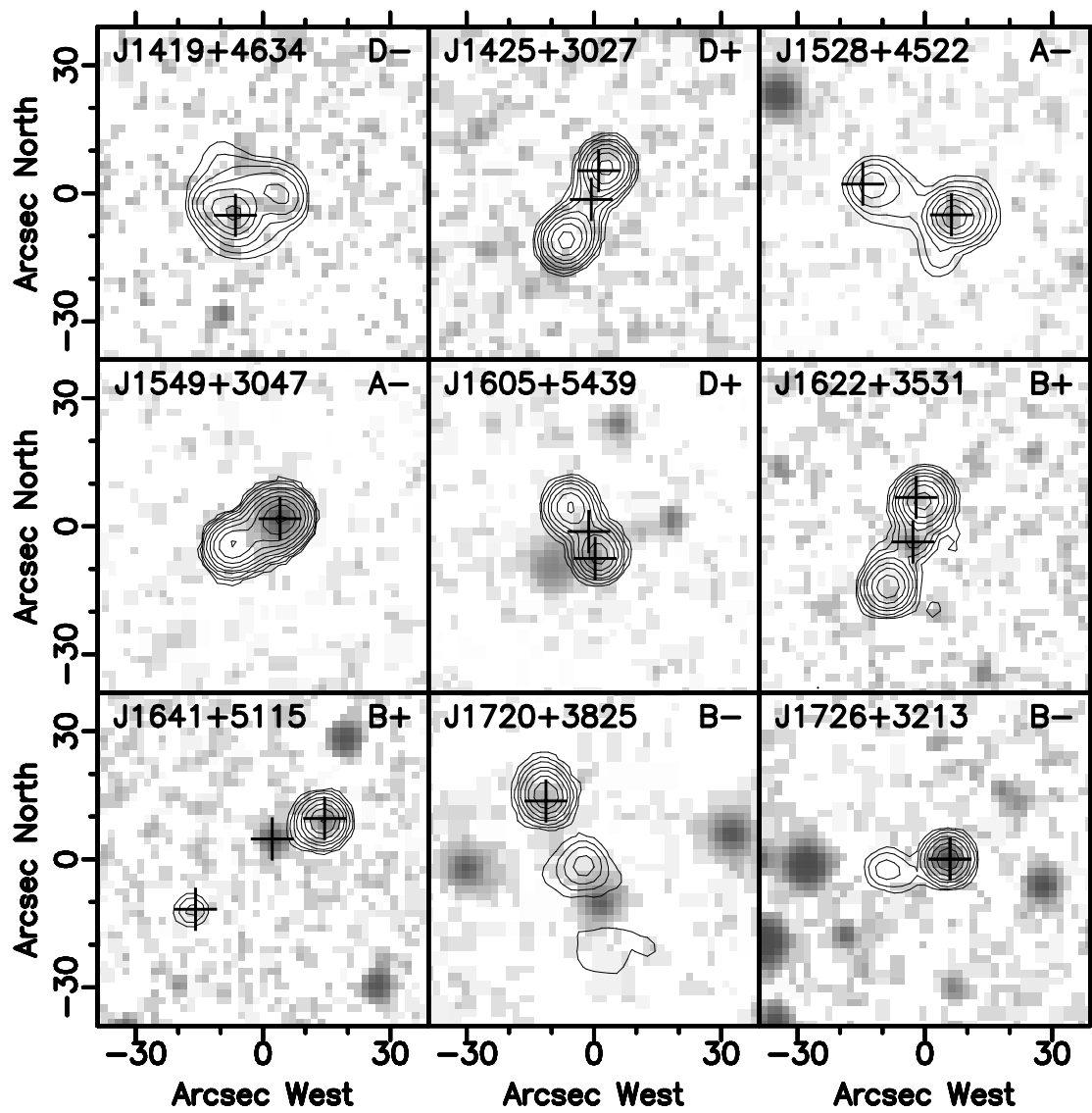


Fig. 1.— More FIRST/DSS maps of the VLA sample.

and the flux densities were scaled to 3C286 (with an assumed flux density of 7.43 Jy). Calibration and mapping followed standard AIPS⁹ procedures, with a single iteration of self-calibration, and a circular convolving beam of $0''.7$ (FWHM), to bring out extended structures. The resulting maps have off-source rms noise levels of ~ 0.1 mJy/beam, close to the thermal noise limit, except for the brightest targets. As expected, most of our radio lobe candidates turned out to be misidentified radio cores, and sometimes presumed lobe components could be resolved into separate radio sources.

Three of the most promising VLA targets were observed at 18 cm using MERLIN (r98a, see Table 4). MERLIN provides sub-arcsecond resolution at lower frequencies, where the steep-spectrum radio lobes are brightest, but is not very sensitive to faint sources. J0823+3906, J0828+3552, and J1622+3531 were each observed eight times in 30 minute scans at intervals of 2–6 hours, to maximize baseline sampling. Standard MERLIN phase calibrators were also observed, and the flux densities and polarizations were calibrated using 3C286 and OQ208, respectively. The data were reduced using the standard MERLIN pipeline, with several iterations of phase self-calibration. The resulting maps have off-source rms noise levels of ~ 0.2 mJy/beam, and an angular resolution of $\sim 0''.25$ (FWHM). MERLIN produced an excellent map of J1622+3531, but in most cases, faint radio lobe structures could be seen.

We obtained optical CCD images for the 12 most promising targets. The objective was to confirm whether candidate lenses are galaxies, and to seek optical counterparts to the radio cores. Observations were acquired when the opportunity arose, so a variety of telescopes and filters were used (see Table 4). The data quality was variable, but the integration times were chosen to permit detection of an $R \sim 24$ mag galaxy. Photometric calibration was achieved, in most cases, by acquiring Landolt (1983) standard star observations during each run, but in a few cases we were forced to calibrate either to spectra or to the APM photometry. In all cases, photometric precision is no better than 0.1 mag on an absolute scale, although relative photometry in each image will be considerably better. The images were reduced using standard IRAF¹⁰ procedures. Over half of the observed candidates could be eliminated as either stars or spurious APM objects, and radio cores were detected for all of the remaining lens candidates (see Figure 2). Two of our targets (J0823+3906 and J1605+5439) were observed through several filters, though time considerations did not permit this for most.

Four of our targets (J0823+3906, J0849+2448, J0958+2947, J1622+3531) were also observed spectroscopically, again using a variety of telescopes as the opportunity arose (see Table 4). The spectra were reduced using standard procedures, and were calibrated by observing flux density standards. All but one of the observations yielded unambiguous redshifts for the targets.

⁹ AIPS (Astronomical Image Processing System) is distributed by the National Radio Astronomy Observatory, which is a facility of the National Science Foundation operated under cooperative agreement by Associated Universities, Inc.

¹⁰ IRAF is distributed by the National Optical Astronomy Observatories, which are operated by the Association of Universities for Research in Astronomy, Inc., under cooperative agreement with the National Science Foundation.

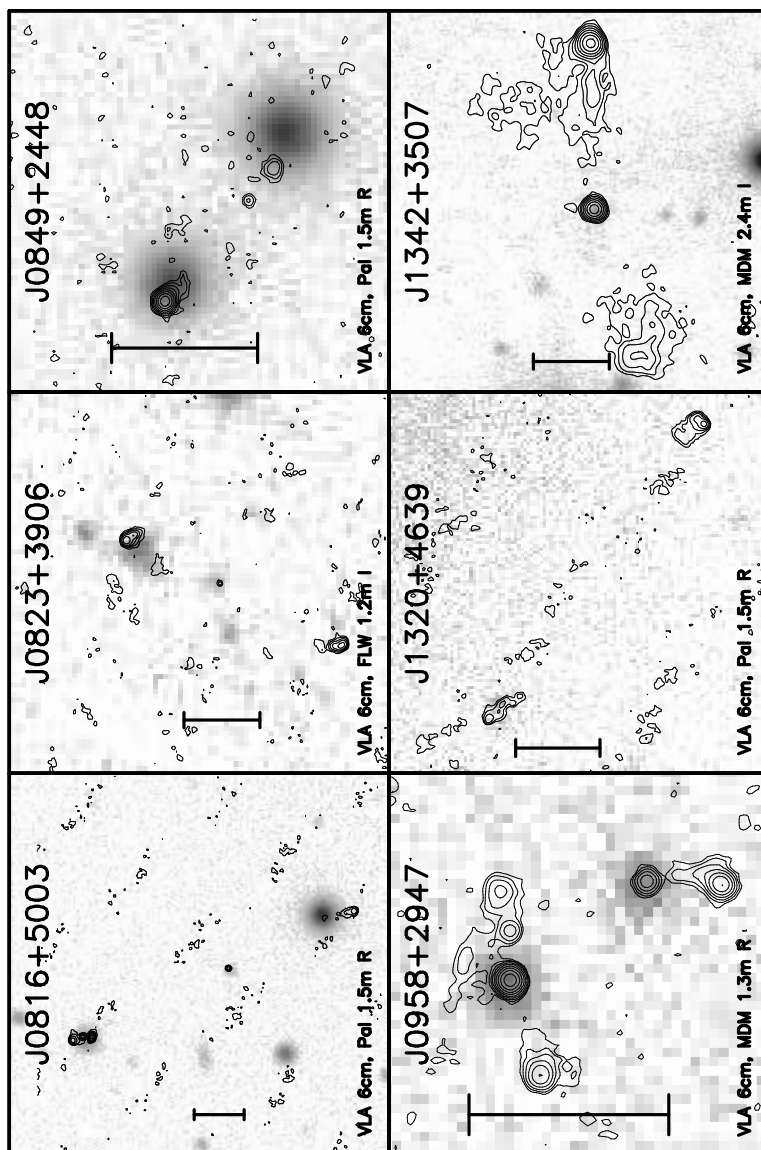


Fig. 2.— VLA and optical images of those candidates with CCD data (see Table 3). The radio contours increase by doubling from twice the off-source map rms (Table 3) with a $0''.7$ beam size (FWHM). The CCD images, shown as logarithmic grey scale, were aligned using APM astrometry. The reference bars are $10''$ long, with $2''$ ends.

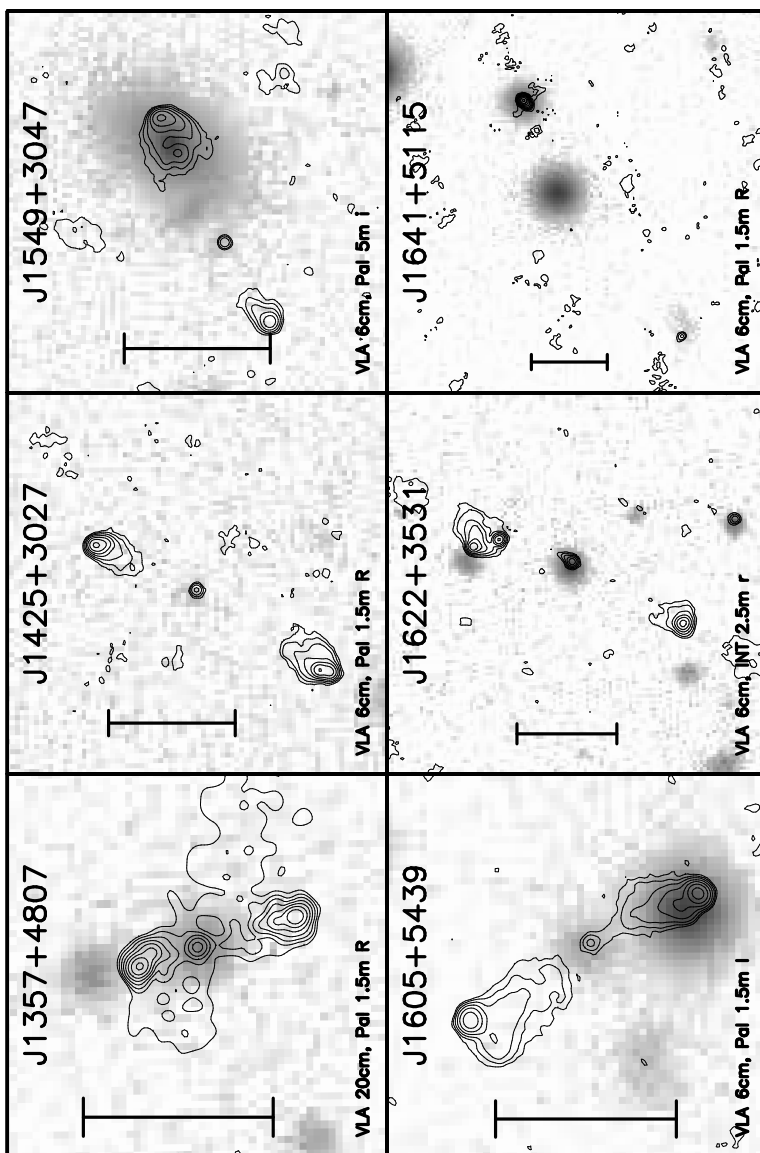


Fig. 2.— More VLA and optical images of CCD targets.

4. Individual Targets

Here, we discuss in detail the twelve candidates which could not be rejected immediately as misidentified radio cores and received CCD observations (see Table 3 and Figure 2). We will refer to observations using the labels in Table 4, and optical photometry of the counterparts will be compared to passively evolving early- and late-type galaxies at various redshifts (for details, see §5 of Lehár et al.2000).

J0816+5003 is lensed. It has three optical counterparts, one on each of the FIRST components, including the central core component (Figure 2). The $R<16$ southern lobe counterpart is stellar, and is too far away from the radio lobe to be of interest to us. However, the northern lobe counterpart, Galaxy 1, lies directly over the northern radio component, which exhibits unusual structure for a radio lobe (Figure 3). Components N1–N3 probably are not an independent FR-type radio source, for two reasons. First, the clear lobe-like appearance of the southern FIRST component leads one to expect a northern radio lobe near Galaxy 1. Second, component N2, which would be the core of such an FR-type source, does not coincide with Galaxy 1’s center, which is $0''.4$ to the South. This arrangement, however, can be readily explained by Galaxy 1 lensing the hot-spot in an ordinary radio lobe into components N1 and N2, leaving N3 distorted but singly imaged (see Figure 3). Moreover, N1 and N2 have the same polarization fraction and orientation (Figure 3), exactly as expected if they are lensed images of the same hot-spot. Matched polarizations are unexpected for the core and jet of an FR-type object (note that the Southern lobe shows similar polarization levels to the N1–N3, but the radio Core is $<5\%$ polarized), and very unusual for distorted-jet hot-spots (e.g. Lonsdale & Barthel 1986a,b). Thus, we conclude that J0816+5003 is lensed. In this case, the image separation of $\Delta\theta=1''.9$ corresponds to an isothermal lens galaxy with a velocity dispersion of $\sim 250 \text{ km s}^{-1}$ if it is at $z\sim 0.4$. Galaxy 1 is slightly extended, with a deconvolved major axis FWHM of $\sim 1''.8$, and an axial ratio of ≈ 0.86 (PA= -64°), and the lens model shown in Figure 3 has been matched to the position and shape of Galaxy 1. The photometry also tentatively favors gravitational lensing: The optical magnitude of Galaxy 1 ($R=19.2$) is consistent with an L_* early-type galaxy at $0.3 < z < 0.5$, and the radio core counterpart ($R=21.7$) is much fainter than Galaxy 1, consistent with its being at a greater distance. To properly confirm this system as lensed, and to provide crucial distance information, multifrequency radio observations and optical spectroscopy are planned.

J0823+3906 is a strong candidate, with a galaxy directly on a radio lobe, but there are no clear lensing signatures. The lobe counterpart (Galaxy 1) is clearly an extended galaxy, with a deconvolved size of $\sim 1''.2$ (FWHM). If we align the optical image so that the optical core coincides exactly with the radio core, the section of the lobe under Galaxy 1 is too faint to allow multiple imaging to be detected in either the VLA or MERLIN maps. Deeper VLA observations (14 min at 20 cm, and 1.7 hr at 6 cm, Figure 4) confirm the flat-spectrum radio core ($\alpha > +0.5$), and find substantial emission near Galaxy 1, but still show no lensing signatures in the steep-spectrum lobe ($\alpha\sim -1$). Lensing would not occur, of course, if the radio source were closer to us than Galaxy 1. Palomar 5 m spectroscopy (Figure 5) could not detect the core, and there were no clear features in

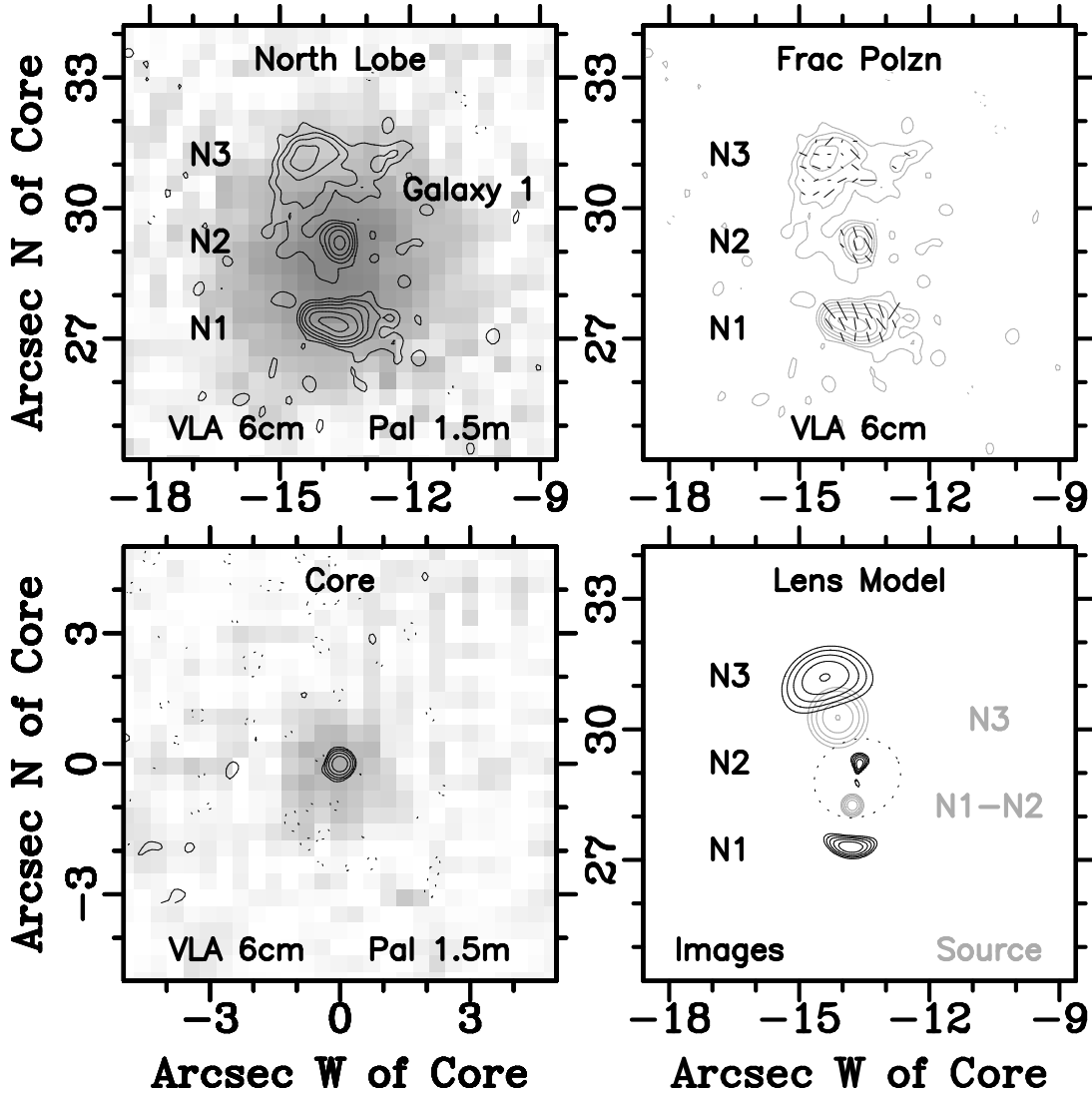


Fig. 3.— VLA maps (r98b) of the core (lower left) and northern lobe components (N1–N3, upper left) for J0816+5003, at high resolution ($0''.35$ FWHM beam size). The optical field (o00b) is shown in logarithmic greyscale, aligned using the core. Radio contours double from twice the off-source rms noise of $0.055 \text{ mJy beam}^{-1}$. The fractional polarization vectors for the northern component (upper right) are parallel to the electric field, and scaled so that one spacing interval corresponds to 33% polarization per beam. A singular isothermal ellipsoid model (lower right), matched to Galaxy 1, shows N1 and N2 as lensed images of a compact hot-spot. The unlensed source contours are shown in grey, while the lensed image contours and critical line (dotted) are in black.

the spectrum of Galaxy 1. However, several dips in the continuum suggest $z \sim 0.3$ as a possibility. V and I band images of J0823+3906 (from o00b), yield $I=19.2$ and $V-I=1.6$ for Galaxy 1. This is consistent with an $L < L_*$ early-type galaxy at $z \sim 0.3$ or an $L \sim L_*$ spiral at $z \sim 0.5$. Either way, Galaxy 1 is not likely to be farther than $z \sim 0.6$. The distance to the radio source is harder to determine, however, although it is much fainter ($I=21.8$) than Galaxy 1. To eliminate lensing for J0823+3906, deeper optical spectroscopy is crucial.

J0849+2448 is not a gravitational lens. There are optical objects close to both radio components, but their $12''.7$ angular separation is greater than the radio component separation, and neither of them falls directly on a radio component. Moreover, both are optically compact, and optical spectra (s98) show them to be local stars (North and South have classes M and G).

J0958+2947 includes two quasars at very different redshifts. This source was first noted in the MG-VLA search (MG0959+3047, Lehar 1991). The VLA map resolves the FIRST components into two separate quasars, each with cores and radio lobes, and there are compact, blue optical counterparts to each core. The optical spectra of the cores (Figure 7) show emission lines corresponding to quasars at high redshift ($z_{north}=2.064$ and $z_{south}=2.744$). J0958+2947 does not show any clear signs of lensing, but the 20 cm map (Figure 6) and the 6 cm map both show a small arc-like extension, N5, about $2''$ northeast of N1. This could either be an unusual structure connected with this quasar, or it could be part of the of the northern lobe associated with S1, which is otherwise not seen. The spectral index ($\alpha < -0.5$) and polarization ($\sim 5\%$) of N5 are typical for a lobe hot-spot. However, the high redshift of the North QSO makes it an inefficient lens for a source at $z=2.744$, so $\Delta\theta \lesssim 0''.4$ for an L_* galaxy. Thus, if N5 is part of the southern radio source, we would not expect to see multiple imaging.

J1320+4639, J1342+3507 (4C+35.30), J1357+4807, and J1425+3027 (MG J1425+3027) are not gravitationally lensed. In each case, deeper optical observations failed to detect any lobe counterpart, so these are likely to be spurious APM detections.

J1549+3047 is the known lens MG J1549+3047 (Lehar et al.1993). This target was selected by our search method, and serves as a clear example of a successful detection. The APM finds a bright counterpart to the western FIRST component. Here, we present a 45 s excerpt of the 6 cm VLA data from Lehar et al.(1993), which gives a lensed ring detection which is comparable to what our other observations should yield. The CCD image clearly detects both the lens galaxy and the core counterpart, and the measured lens redshift ($z=0.111$, Lehar et al.1993) is much less than the typical radio source redshift. Moreover, corresponding parts of the lensed ring have matching spectral index and fractional polarization (Lehar et al.1993).

J1605+5439 is not lensed. The southern lobe counterpart has a stellar profile, and there is no evidence of lensing in the radio lobe. Moreover, the photometry (from o00b) of the lobe counterpart ($I=16.8$, $V-I=3.2$) is inconsistent with a normal galaxy at any redshift. The core counterpart ($I=20.3$, $V-I=1.6$), however, is consistent with a galaxy at $z > 0.3$.

J1622+3531 has nearby galaxy in front of a distant lobe, but our observations failed to detect

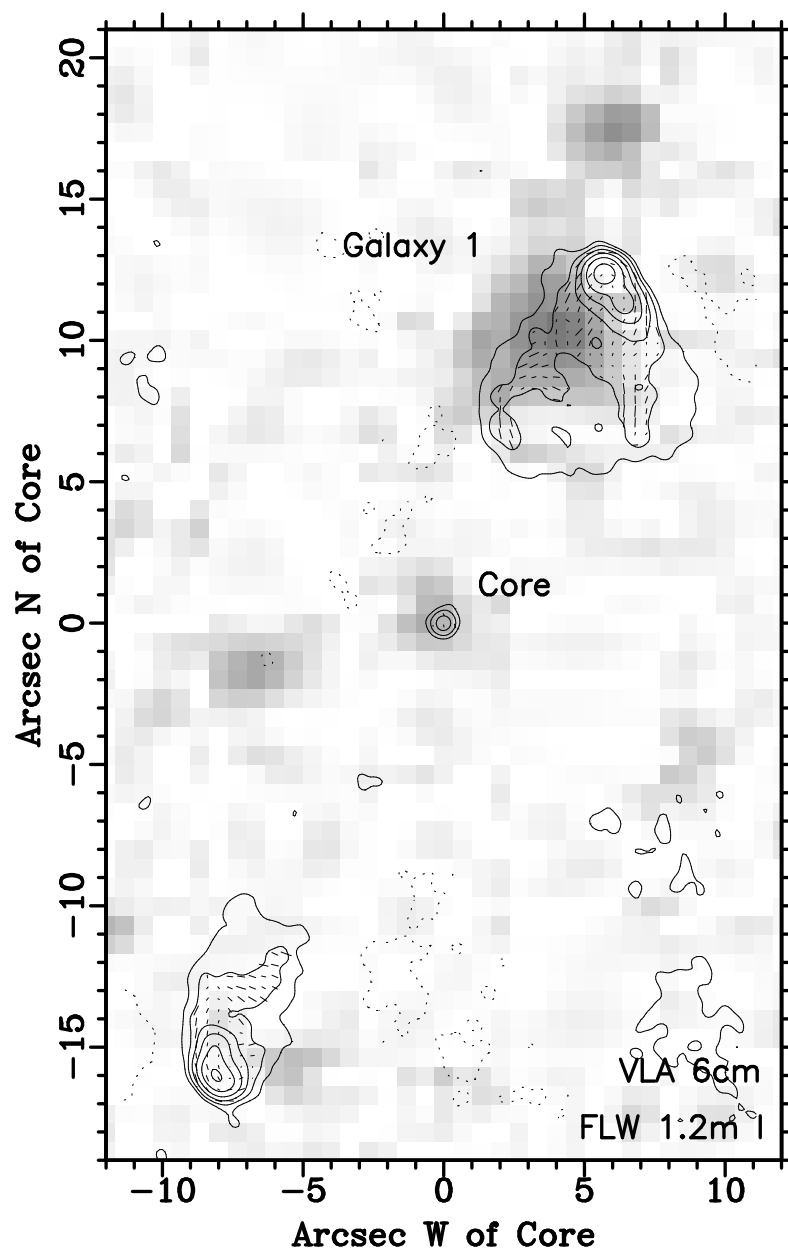


Fig. 4.— Deeper VLA map of J0823+3096 (r99) at 6 cm (1.7 hr). The optical field (o00a) is shown in logarithmic grey scale, aligned to the radio using the core. The radio contours double from twice the off-source rms noise of $0.062 \text{ mJy beam}^{-1}$, for a beam FWHM of $\sim 0''.7$. The fractional polarization is shown as vectors parallel to the electric field, scaled so that one spacing interval corresponds to 33% polarization per beam.

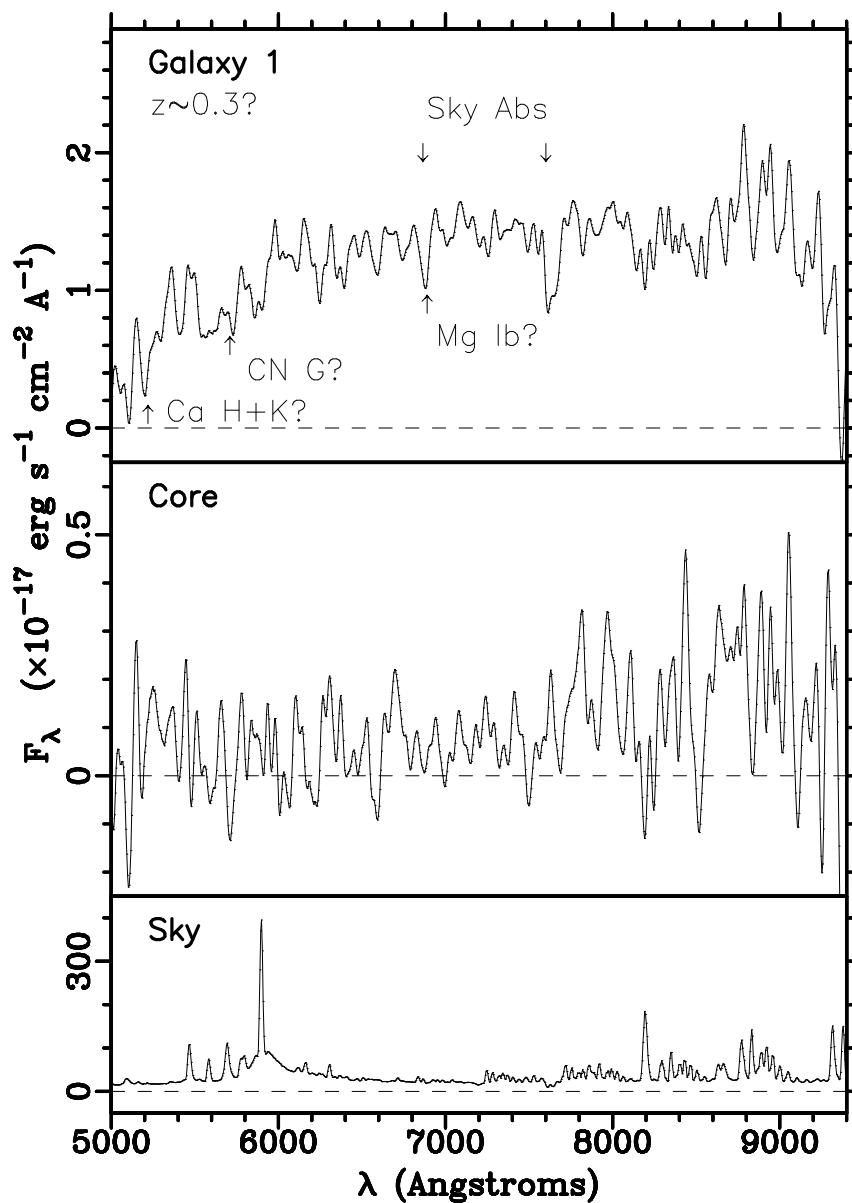


Fig. 5.— Optical spectra of the J0823+3096 system from a 1.2 hr observation (s00) on the Palomar 5 m telescope. Spectra are presented for the Galaxy counterpart to the radio lobe, the radio core counterpart, and the sky level during the observation. The target spectra have been smoothed to $\sim 20 \text{ \AA}$ resolution (FWHM). Possible spectral features at $z=0.33$ are shown for Galaxy 1, based mostly on the continuum shape. The core was barely detected.

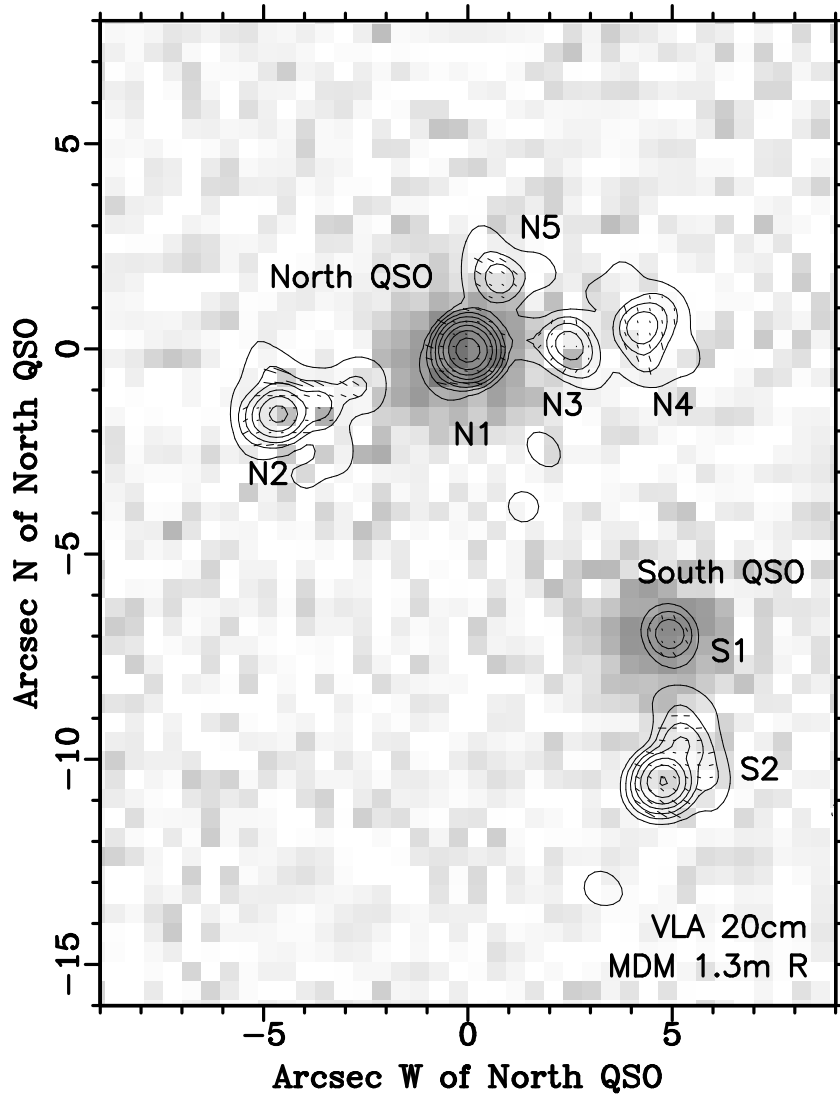


Fig. 6.— VLA A-array map of J0958+2846 at 20 cm (r90b, 15 min) with radio components labeled N1–N5 and S1–S2. The optical field (o90) is in logarithmic grey scale, aligned using the North QSO. The radio map is super-resolved to match the $0''.7$ resolution of the 6 cm observation (Figure 2), and contours double from twice the off-source rms noise of $0.21 \text{ mJy beam}^{-1}$. Fractional polarization vectors are parallel to the electric field, and are scaled so that the vector spacing corresponds to 33% per beam.

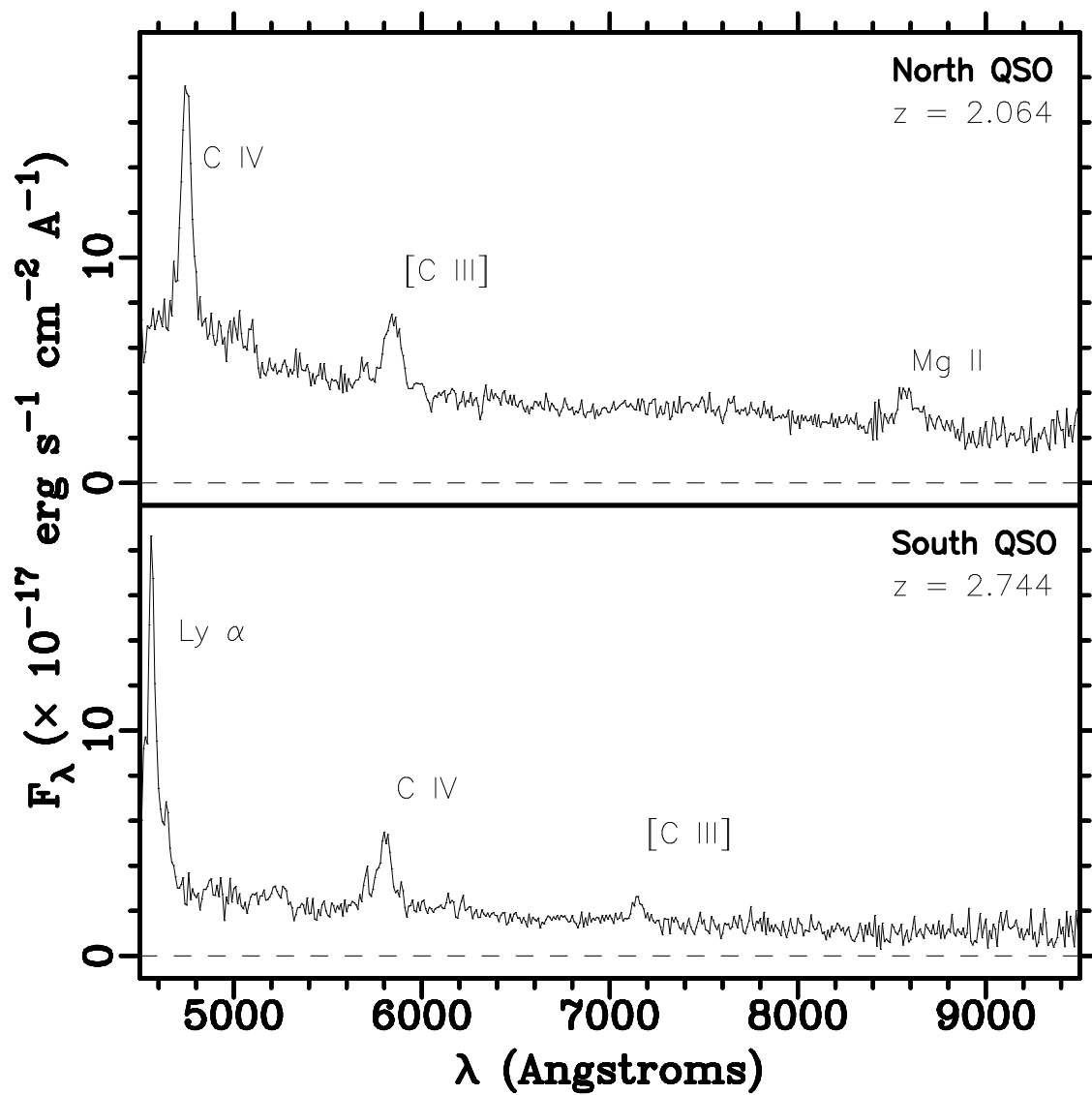


Fig. 7.— Optical spectra for J0958+2846 from a 10 min Palomar 5 m observation (s90). Both objects show strong emission lines corresponding to high redshift quasars.

lensing signatures. The VLA and MERLIN (Figure 8) maps show the northern lobe to be broken into two steep-spectrum ($\alpha \sim -1$) subcomponents, N1 and N2, and there are optical counterparts to both the northern lobe and the inverted spectrum radio core ($\alpha = +0.5 \pm 0.1$). Galaxy 1, at $z = 0.32$, is extended (deconvolved FWHM $\sim 0''.9$) and at lower redshift than the Quasar, at $z = 1.47$ (Figure 9). We can roughly reproduce the N1,N2 configuration using a simple lens model (Figure 8), but the lens must lie between N1 and N2, where no optical counterpart is found. Moreover, the spectral indices ($\alpha_{N1} \approx -0.7$, $\alpha_{N2} \approx -0.2$) and fractional polarizations (Figure 8) of N1 and N2 are inconsistent. Thus we conclude that the morphology of the northern lobe is probably due to a bent radio jet (e.g. Lonsdale & Barthel 1986a,b). Galaxy 1 *must be* lensing the more distant radio lobe, but it is probably just distorting the intrinsic shape. Galaxy 1 is 2–3 mag fainter than an L_* early-type galaxy, with an expected image separation of $\sim 0''.7$, so we might find a faint lensed image of the northern hot-spot near Galaxy 1 in deeper radio observations.

J1641+5115 is not a gravitational lens. There are three APM counterparts, one each for the two FIRST components, and one between them. The VLA map shows the western radio component to be the core, and the eastern counterpart falls $2''$ away from the eastern radio source.

5. Conclusions

Our initial search for lensed radio lobes using the FIRST survey and the APM catalog has produced two lenses (J0816+5003, J1549+3047), one of which is the known lens MG J1549+3047 (Lehar et al. 1993). Two more lens candidates (J0823+3906, J1622+3531), have galaxies superposed on radio lobes, but show no evidence of multiple imaging. One of our targets (J0958+2947) is a pair of quasars in close projection.

Our search method is highly efficient, even assuming that all of our unconfirmed candidates are not lensed. The FIRST/APM search found 2 lensed systems, using only 33 VLA observations. Thus 6% of our VLA targets are lensed, compared to a success rate of only 0.2% for other radio lens searches, and $< 1\%$ for bright quasar searches. This gain in efficiency results from combining optical and radio surveys to find radio sources with unusual optical counterparts that favor lensing. There are many more lensed radio lobes to be found in this way. Since our initial search, the FIRST survey has trebled in size, covering $\sim 80\%$ of the planned $\sim 10,000$ square degrees. Thus, we should discover ~ 10 lensed lobes using the FIRST/APM comparison in the very near future.

The sample can be expanded with fainter optical catalogs. The POSS-I plates detect only $\sim 30\%$ of known lens galaxies, so considerable gains can be made with deeper optical surveys. We are currently extending our search using the POSS-II survey (Djorgovski et al. 1998), which should find *at least* $\sim 50\%$ more lens galaxies than the APM, leading to ~ 15 expected lensed lobes. Moreover, two thirds of the APM lobe counterparts turned out to be stellar or spurious in CCD images. This suggests that selection based on a higher quality optical survey, such as the Sloan Digital Sky Survey (Gunn & Knapp 1992), could treble the search efficiency.

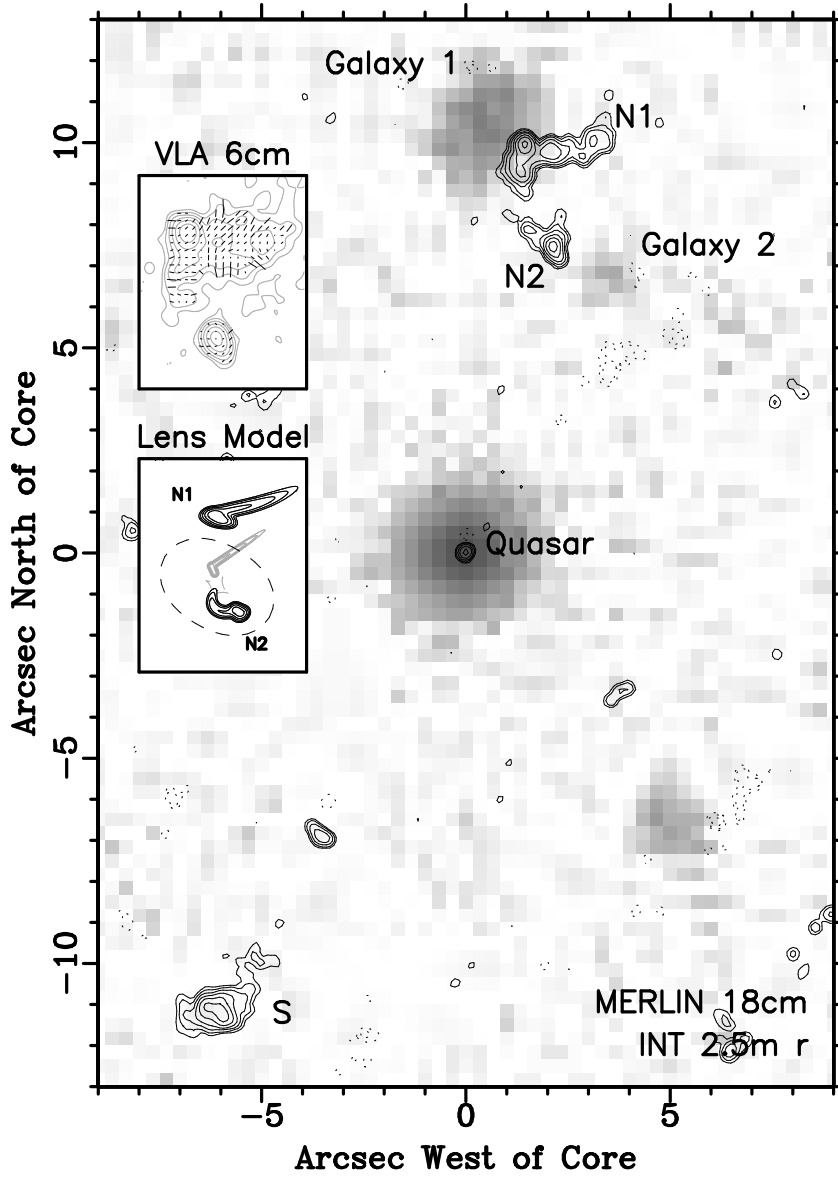


Fig. 8.— MERLIN map of J1622+3531 (r98a, 4 hr) at 18 cm. The optical field (o99b) is shown in logarithmic grey scale, aligned using the Quasar and radio core. Radio contours double from twice the off-source rms noise of $54 \mu\text{Jy beam}^{-1}$, for a beam size of $0''.25$ (FWHM). The upper inset shows the VLA 6 cm map (r98b) of the northern radio lobe at $0''.35$ resolution (rms noise $82 \mu\text{Jy beam}^{-1}$), with fractional polarization vectors scaled so that 33% per beam corresponds to the vector spacing. The lower inset shows a singular isothermal ellipsoid lens model, with N1 and N2 as lensed images of each other. The unlensed source contours and the caustic (dashed) are shown in grey, and the lensed image contours and critical line (dashed) are in black.

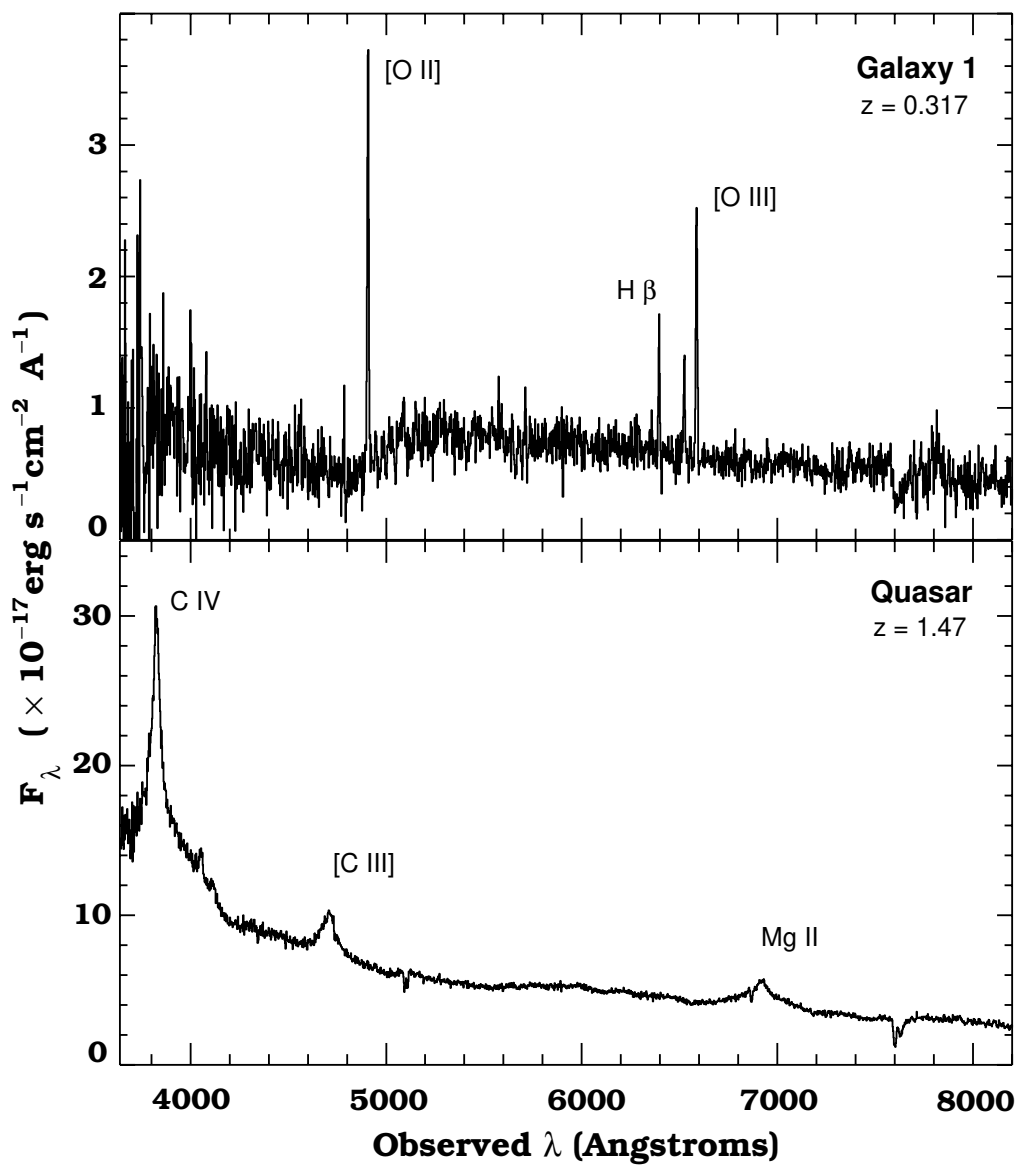


Fig. 9.— Optical spectra for J1622+3531, from a 15 min observation using the Keck II telescope (s99). The radio core is a quasar at high redshift, and the brighter lobe counterpart (Galaxy 1) is a lower redshift star-forming galaxy.

Even greater gains are possible as radio telescopes improve. We had to reject 92% of our FIRST/APM candidates because the FIRST components were too faint for easy VLA mapping. Thus, as the VLA upgrades to larger bandwidth, and once higher resolution 20 cm observations are possible using the VLA-Pie Town link or the extended A+ array, hundreds of lensed lobes could be found in the Northern sky.

6. Appendix: Collapsing the FIRST catalog

Many radio sources exhibit complex morphology (e.g., doubled-lobed, FR-type objects), and often include several components in the FIRST catalog. Thus, it is useful to first “collapse” the FIRST catalog into component groups for each source. The collapsing procedure we employ here is based on the circular overdensity algorithm of Buchalter (1999), which has been used to systematically identify and characterize large numbers of multi-component radio sources in the FIRST Survey (e.g. Blanton et al.1997; Buchalter et al.1998).

First, we morphologically classify individual FIRST components and collect them into associated groupings. Components classified as sidelobes are removed from the radio catalog and remaining components are classified as “extended” or “compact”, depending on whether the major axis of the fitted Gaussian profile exceeds $2''$. For compact (extended) components, the radio flux is taken to be the listed peak (integrated) flux (see Becker, White, & Helfand, 1995). Starting at the coordinates of the first catalogued component in a source, the program looks for other components within a fixed search radius, R . If another component is found, the average position is determined, and the search continues from the new average position. The process is repeated until no additional components are found within a distance R of the last search center.

For each component grouping, an estimated probability of random association is calculated to determine whether the grouping qualifies as a single radio source. Denoting the number of sources found in a given iteration by N , the largest separation between the original source and any other by d_1 , and the flux of the faintest source in a given iteration by F_{\min} , the program calculates the probability of obtaining $N - 1$ sources all with fluxes $\geq F_{\min}$ and within a distance d_1 of the original source, based on counting statistics and on the measured two-point correlation function of the FIRST Survey¹¹ (Cress et al.1996). If the observed configuration has a small probability, P ,

¹¹ The two-point correlation function, ξ_2 , gives only the excess probability of finding *pairs* separated by a given distance. Inasmuch as the observed clustering is weak, i.e., $\xi_2 \ll 1$, we may conservatively take ξ_2 to be an upper limit for the excess probability of finding configurations of triples, quadruples, and so on, since higher-order n -point correlation functions, ξ_n , scale roughly as $\xi_n \propto \xi_2^{n-1}$ in the quasi-linear regime (Fry 1984). According to Cress et al.(1996) the measured two-point correlation function for FIRST, once the fragmentation of multicomponent sources (such as FR-type objects) is accounted for, extrapolates to a value of unity only at a scale of about $20''$, so that using ξ_2 as an upper limit to the higher-order n -point correlation functions should be valid at all but the smallest scales we consider. Even if two components are separated by only the survey resolution limit of $\sim 5''$, and the two-point function exhibited no turnover at such small scales, we would only find $\xi_2 \approx 4$, thus perhaps slightly

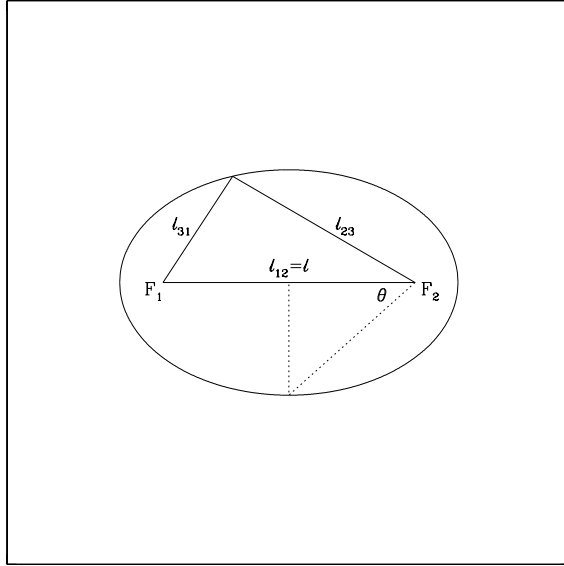


Fig. 10.— Illustration of the definition for the bending angle, θ . The triangle formed by three given radio components has sides $\ell = \ell_{12} > \ell_{23} > \ell_{31}$ and defines an ellipse with foci F_1 and F_2 . The angle θ is given by $\theta = \arccos \frac{\ell_{12}}{\ell_{23} + \ell_{31}}$.

of random association, compared to a chosen significance cutoff, the components are considered to be associated with a single source. Once a component is identified with a source, it is no longer considered by the collapse routine in any subsequent searches. If, however, the random association probability exceeds the cutoff, such that no association is found, the program initiates a new search centered at the position of the next catalogued FIRST component. The individual components in the “failed” search attempt are still considered as candidates for collapse in later search iterations.

Each source is then characterized by its component properties and a set of parameters which can vary with the number of components N . For all sources, the average position and aggregate radio flux of all components are tabulated, as well as the flux of the brightest component. For pairs ($N=2$) the morphology is characterized as “both extended”, “both compact”, or “one compact/one extended” components. For the case of “both extended” components, the difference in position angle between the two components is calculated as a measure of the alignment.

For triples ($N=3$), we identify the “core” component as that which is not an endpoint of the longest leg, ℓ , of the three triangle legs formed (see Figure 10). Denoting the three legs by ℓ_{12} , ℓ_{23} , and ℓ_{31} , such that $\ell = \ell_{12} > \ell_{23} > \ell_{31}$, we calculate a symmetry factor, S , given by ℓ_{31}/ℓ_{23} , as well

overestimating the number of collapsed sources at the very smallest scales.

as a bending angle, θ , defined geometrically by $\theta = \arccos \frac{\ell_{12}}{\ell_{23} + \ell_{31}}$. Thus, θ is the angle defined by going from one focus to the other to the endpoint of the semi-minor axis of an ellipse whose foci (F_1, F_2) are separated by a distance ℓ_{12} and whose major axis is equal to $\ell_{23} + \ell_{31}$. Requiring that θ be less than some chosen value, θ_c , ensures that the “core” is located within the ellipse defined by θ_c . Obviously, the requirement that $\ell_{12} > \ell_{23} > \ell_{31}$ implies that $\theta < 60^\circ$. In addition, the morphology of the “core” component and the “lobe” components are noted for triples.

Associations with more than three FIRST components are termed “multiples.” For these sources, we find the largest separation, ℓ , between any two components, and take the bending angle, θ , to be the maximum value obtained (in the manner described above) from all triangles in which one side is given by ℓ . Furthermore, if one or more components lie within a distance $\ell/4$ of the average position, the program identifies as a “core” that component nearest to the center; otherwise, no core is identified.

Acknowledgements: We are grateful to Bob Becker, Emilio Falco, Mike Irwin, Don Schneider, and Ion Yadigaroglu for providing optical spectra and CCD images. It is also a pleasure to thank David Helfand and George Djorgovski for many helpful comments. CSK is supported by the Smithsonian Institution. This work was partially supported by NASA/HST grants GO-7495 and GO-7887, and by NSF/AST-9802732.

REFERENCES

- Baugh, C.M., & Efstathiou, G.; 1993, MNRAS, 265, 145
- Becker, R.H., White, R.L., & Helfand, D.J.; 1995, ApJ, 450, 559
- Blandford, R.D., Narayan, R.; 1992, ARA&A, 30, 311
- Blanton, E.L., Helfand, D.J., Becker, R.H., Gregg, M.D., White, R.L.; 1997, BAAS; 191, 106.12
- Buchalter, A.; 1999, PhD Thesis
- Buchalter, A., Helfand, D.J., Becker, R.H., White, R.L.; 1998, ApJ, 494, 503
- Burke, B.F., Conner, S.R., Hewitt, J.N., Lehár, J.; 1993, in “Sub-Arcsecond Radio Astronomy”, Eds R.J. Davis, R.S. Booth (Cambridge:CUP), p.123
- Cress, C.M. & Kamionkowski, M.; 1998, MNRAS, 297, 486
- Cress, C.M., Helfand, D.J., Becker, R.H., Gregg, M.D., White, R.L.; 1996, ApJ, 473, 7
- Djorgovski, S., de Carvalho, R., Gal, R., et al.; 1998, in “New Horizons from Multi-Wavelength Sky Surveys”, IAU Symp., 179, 424.

- Fanaroff, B.L. & Riley, J.M.; 1974, MNRAS, 167, 31
- Falco, E.E., Impey, C.D., Kochanek, C.S., Lehár, J., McLeod, B.A., Rix, H.-W., Keeton, C.R., Muñoz, J.A., Peng, C.Y.; 1999, ApJ, 523, 617
- Fry, J.N.; 1984, ApJ, 279, 449
- Fukugita, M., Turner, E.L., 1991, MNRAS, 253, 93
- Gunn, J., & Knapp, G.; 1992, in “Sky Surveys, Protostars to Protogalaxies”, ed. T. Soifer, ASP Conf., 43, 267.
- Hewitt, J.N., Turner, E.L., Schneider, D.P., Burke, B.F., Langston, G.I.; 1988, Nature, 333, 537
- Irwin, M., Maddox, S., & McMahon, R.; 1994, Spectrum, 2, 14.
- Jackson, N., Nair, S., Brown, I.; 1998, in “Observational Cosmology from Radio Surveys” (Dordrecht:Kluwer), ASSL, 226, 333.
- Keeton, Kochanek, C.S., Seljak, U.; 1997, ApJ, 482, 604
- Keeton, Kochanek, C.S., Falco, E.E.; 1998, ApJ, 509, 561
- Keeton, C.R., Falco, E.E., Impey, C.D., Kochanek, C.S., Lehár, J., McLeod, B.A., Rix, H.-W., Muñoz, J.A., Peng, C.Y.; 2000, to appear in ApJ, astro-ph/0001500
- Kochanek, C.S. & Lawrence, C.R.; 1990, AJ, 99 1700
- Kochanek, C.S.; 1993a, ApJ, 417, 438
- Kochanek, C.S.; 1993b, ApJ, 419, 12
- Kochanek, C.S.; 1995, ApJ, 445, 559
- Kochanek, C.S.; 1996a, ApJ 466, 637
- Kochanek, C.S.; 1996b, ApJ, 473, 595
- Kochanek, C.S., Narayan, R.; 1993, ApJ, 401, 461
- Kochanek, C.S., Falco, E., Impey, C.D., Lehár, J., Rix, H.-W., Keeton, C.R., Muñoz, J.A., Peng, C.Y.; 2000, ApJ, in press, astro-ph/990901
- Landolt, A.U.; 1983, AJ, 88, 853
- Langston, G., Schneider, D., Conner, S., et al.; 1989, AJ, 97, 1283.
- Lehár, J.; 1991, MIT Ph.D. Thesis
- Lehár, J., Langston, G.I., Silber, A., Lawrence, C.R., Burke, B.F.; 1993, AJ, 105, 847

- Lehár, J., Falco, E.E., Impey, C.D., Kochanek, C.S., McLeod, B.A., Rix, H.-W., Keeton, C.R., Muñoz, J.A., Peng, C.Y.; 1999, to appear in *ApJ*, astro-ph/9909072
- Lonsdale, C.J., Barthel, P.D.; 1986a, *AJ*, 92, 12
- Lonsdale, C.J., Barthel, P.D.; 1986b, *ApJ*, 303, 617
- Maddox, S.J., Efstathiou, G., Sutherland, W.J., Loveday, J.; 1990, *MNRAS*, 243, 692
- McMahon, R., & Irwin, M.; 1992, in “Digitised Optical Sky Surveys”, ed. MacGillivray & Thompson, *Kluwer Astroph. & Space Sci.*, 174, 417.
- Patnaik, A.R., Browne, I.W.A., Wilkinson, P.N., Wrobel, J.M.; 1992, *MNRAS*, 254, 655
- Schneider, P., Ehlers, J., Falco, E.E.; 1992, “Gravitational Lenses”, (Springer:Berlin)
- Turner, E.L; 1990, *ApJ*, 365, 43

Table 1. Lens Candidate Optical Classification

APM Class	Lensed Lobe Candidates	FIRST Counterparts	APM Objects	Comments
A+/A-	47%	55%	21%	red, extended
B+/B-	33%	40%	58%	red, compact
C+/C-	6%	2%	10%	blue, extended
D+/D-	14%	3%	11%	blue, compact

Note. — Here, ‘red’ means that the APM $B-R > 0.5$ mag, and ‘extended’ means that the APM object classification was either ‘galaxy’ or ‘merged’, versus ‘stellar’ or ‘noise-like’. The optical morphology was taken from the band in which the APM counterpart appeared brighter. The sign (+/-) indicates whether a separate counterpart to the the presumed radio core was (present/absent). APM statistics are based on $\sim 13,400$ $R > 15$ objects from 8 arbitrarily chosen $10'$ fields.

Table 2. Lensed Lobe Candidate Selection Criteria

Criterion	Comments
Radio Sources	
Component fluxes > 3 mJy	To ensure detection in radio follow-up.
Brightest > 10 mJy	To enable self-calibration in radio follow-up.
Separation $< 60''$	Search radius to associate any 2 components.
Max. separation of $90''$	For triple and multiple FIRST sources.
Random assoc. prob. $< 10\%$	To ensure significant component grouping.
Symmetry factor $S > 0.5$	For triples, to eliminate chance associations.
Bending angle $\theta < 30^\circ$	For triples and multiples, to eliminate chance assoc.
Small Lobes	Reject if radio lobe size $> 10''$, to ensure contrast.
Optical Counterparts	
Detected in POSS-I	Optical objects brighter than $R \sim 20$ or $B \sim 22$.
Coincides with lobe	Within $2''$ of the peak, or inside the FIRST FWHM ellipse.
Not likely host	Eliminate cases of one counterpart to both lobes in a double.
Not likely host	Reject if only one APM counterpart, on a compact component.
VLA sample	
APM close to lobe's peak	Reject if APM farther than $2''$ from fitted peak.
FIRST flux > 100 mJy	To distinguish lobes/cores in < 30 min (78 candidates).
Best visual ranking	To accommodate limited observing time (33 targets).

Note. — Before collapsing the FIRST sources, we eliminated VLA sidelobes, and classified each FIRST component as compact (major axis FWHM $< 2''$) or extended. We identified the “core” position of a collapsed source to be the centroid for doubles, or the middle component position for triples. For multiples, we located the component closest to, and within $\ell/4$ of, the centroid; or simply used the centroid if no components were close enough.

Table 3. VLA Sample of Lensed Lobe Candidates

FIRST			APM			VLA				CCD				Notes	
J2000	Coordinates	mJy	R	B	class	exp	λ	noise	obs	exp	filt	lim	seeing		obs
07:12:29.7	+33:33:47	214	15.8	18.7	A-	9	6.0	0.33	r98b				...		not lobe
07:41:43.3	+33:35:39	137	18.4	>22	B-	14	6.0	0.09	r98b				...		not lobe
08:09:13.7	+31:22:21	176	17.6	19.3	A-	8	6.0	0.13	r98b				...		not lobe
08:16:37.4	+50:03:39	121	18.7	>22	A-	18	6.0	0.12	r98b	55	R	25.9	1''8	o00b	LENS
08:23:24.2	+39:06:26	110	19.4	>22	A-	18	6.0	0.09	r98b	80	I	27.2	1''6	o00a	lens?
08:24:59.4	+47:16:42	137	19.0	21.7	A-	14	6.0	0.12	r98b				...		not lobe
08:28:22.7	+35:52:59	146	19.1	20.2	B-	13	6.0	0.07	r98b				...		not lobe
08:49:26.9	+24:48:55	134	16.4	18.9	B-	9	6.0	0.07	r98b	35	R	25.4	1''8	o00b	two stars
09:04:16.1	+42:38:04	1112	19.9	21.6	B-	4	6.0	0.47	r98b				...		not lobe
09:04:54.8	+48:25:53	114	19.5	20.1	B-	14	6.0	0.07	r98b				...		not lobe
09:58:58.8	+29:47:59	138	19.5	19.2	D-	21	6.0	0.07	r90b	20	R	24.2	1''7	o90	lens?
10:36:42.0	+25:02:32	119	17.5	18.0	B-	14	6.0	0.06	r98b				...		not lobe
11:10:43.2	+45:58:02	178	>20	20.7	D-	9	6.0	0.09	r98b				...		not lobe
12:04:58.9	+49:40:26	155	17.6	21.1	A-	4	6.0	0.16	r98b				...		not lobe
12:21:19.0	+24:33:25	362	19.9	>22	B-	6	6.0	0.14	r98b				...		not lobe
12:21:27.6	+50:48:53	218	19.6	20.4	B-	9	6.0	0.08	r98b				...		not lobe
12:36:38.2	+28:40:30	112	18.3	>22	A+	13	6.0	0.07	r98b				...		not lobe
13:20:05.6	+46:39:43	102	19.8	>22	B-	14	6.0	0.10	r98b	80	R	26.5	1''4	o00b	not galaxy
13:23:02.6	+29:41:33	714	>20	21.2	D-	2	3.6	0.56	r90a				...		not lobe
13:37:07.6	+48:58:01	163	16.6	18.7	A-	9	6.0	0.18	r98b				...		not lobe
13:42:31.6	+35:07:11	380	19.9	>22	B-	5	6.0	0.24	r84	60	I	24.8	1''2	o99a	not galaxy
13:53:26.4	+57:25:50	214	19.0	20.9	B-	2	20.	0.23	r91a				...		not lobe
13:57:30.5	+48:07:41	158	19.7	>22	A+	2	20.	0.22	r91a	60	R	26.4	1''3	o00b	not galaxy
14:17:58.4	+40:51:56	105	19.5	21.5	B-	17	6.0	0.07	r98b				...		not lobe
14:19:46.0	+46:34:27	141	19.1	19.6	D-	2	20.	0.24	r91a				...		not lobe
14:25:01.2	+30:27:14	223	>20	22.0	D+	7	6.0	0.13	r95	80	R	25.8	1''3	o00b	not galaxy
15:28:41.9	+45:22:19	153	19.0	19.8	A-	12	6.0	0.08	r98b				...		not lobe
15:49:12.7	+30:47:14	877	15.8	18.7	A-	1	6.0	0.48	r91b	5	i	25.6	0''9	o91	LENS
16:05:38.4	+54:39:23	127	>20	21.4	D+	25	6.0	0.08	r98b	60	I	25.4	1''9	o00b	not galaxy
16:22:29.8	+35:31:27	218	19.9	21.7	B+	18	6.0	0.15	r98b	5	r	27.0	1''0	o99b	lens?
16:41:57.4	+51:15:36	138	18.5	19.1	B+	19	6.0	0.14	r98b	55	R	25.7	2''2	o00b	not lobe
17:20:09.6	+38:25:41	152	18.9	21.4	B-	6	6.0	0.13	r98b				...		not lobe
17:26:35.6	+32:13:22	121	17.0	17.6	B-	17	6.0	0.10	r98b				...		not lobe

Note. — Obs labels refer to Table 4, and exposure times are in minutes. Noise estimates are off-source rms levels in mJy/beam for VLA, and 1σ stellar detection limits for CCD observations. The notes summarize the outcome of this search, where “not galaxy” means a stellar counterpart with no evidence for lensing, or a spurious APM detection.

Table 4. Observations of the VLA Sample

Label	Date	Description	Reference (Observer)
Radio Observations			
r84	1984.11.26	VLA:A, 6 cm, archival	(J. Condon)
r90a	1990.05.03	VLA:A, 3.6 cm, archival	Burke et al.1993 (AB568)
r90b	1990.05.07	VLA:A, 6&20 cm, archival	Lehár 1991 (AB456)
r91a	1991.06.28	VLA:A, 20 cm, archival	(S. Rawlings, AR250)
r91b	1991.08.02	VLA:A, 6 cm, archival	Lehár et al.1993 (AB611)
r95	1995.06.26	VLA:A, 6 cm, archival	(E. Falco, AF293)
r98a	1998.04.19→20	^a MERLIN+Lovell, 18 cm, 24 hr	(J. Lehár, MN/L/98A/33)
r98b	1998.05.26	VLA:A, 6 cm, 8 hr	(J. Lehár, AL434)
r99	1999.09.06	VLA:A, 6&20 cm, 1 hr	(J. Lehár, AL434)
Optical CCD observations			
o90	1990.03.20	^b MDM 1.3 m, archival	Lehár 1991
o91	1991.09.04	^c Palomar 5 m, archival	Lehár et al.1993
o99a	1999.01→02	^b MDM 2.4 m	(I. Yedigarglu)
o99b	1999.07.18	^d INT 2.5 m	(M. Irwin)
o00a	2000.01.13	^e FLW 1.2 m	(E. Falco)
o00b	2000.02→03	^c Palomar 1.5 m	(A. Buchalter)
Optical Spectroscopy			
s90	1990.05.16	^c Palomar 5 m, 4-shooter, archival	(D. Schneider)
s98	1998.03.02	^d INT 2.4 m, IDS	(M. Irwin)
s99	1999.07.27	^f Keck II 10 m, LRIS	(R. Becker)
s00	2000.02.03	^c Palomar 5 m, Norris	(A. Buchalter)

^aMERLIN is operated by the University of Manchester as a national facility of the Particle Physics & Astronomy Research Council (PPARC), in the United Kingdom.

^bThe MDM Observatory is operated by a consortium of the University of Michigan, Dartmouth College, and Columbia University.

^cThe Palomar observatory is operated by the California Institute of Technology.

^dThe Isaac Newton Telescope (INT) is operated on the island of La Palma by the Isaac Newton Group in the Spanish Observatorio del Roque de los Muchachos of the Instituto de Astrofísica de Canarias.

^eThe Fred Lawrence Whipple Observatory on Mt Hopkins, AZ, is operated by the Smithsonian Astrophysical Observatory.

^fThe W.M. Keck Observatory is operated as a scientific partnership among the California Institute of Technology, the University of California and the National Aeronautics and Space Administration. The Observatory was made possible by the generous financial support of the W.M. Keck Foundation.